Black phosphorus and its isoelectronic materials

Fengnian Xia[1]*, *Han Wang*[2]*, *James C. M. Hwang*[3], *A. H. Castro Neto*[4,5] *and Li Yang*[6]*

Abstract | The family of 2D and layered materials has been expanding rapidly for more than a decade. Within this large family of hundreds of materials, black phosphorus and its isoelectronic group IV monochalcogenides have a unique place. These puckered materials have distinctive crystalline symmetries and exhibit various exciting properties, such as high carrier mobility, strong infrared responsivity, widely tunable bandgap, in-plane anisotropy and spontaneous electric polarization. Here, we review their basic properties, highlight new electronic and photonic device concepts and novel physical phenomena and discuss future directions.

Orthorhombic black phosphorus (BP), the most stable allotrope of phosphorus, is a semiconductor that was first synthesized more than a century ago[1]. BP was previously explored as a bulk semiconductor in the 1980s[2]. Complementing the research on graphene and other 2D materials[3–16], BP was rediscovered as a 2D and thin-film material[17–25], leading to many discoveries of interesting physical phenomena such as perfectly linearly polarized light emission from monolayer and few-layer forms, spin-split Landau levels in the quantum Hall regime, tunable topological and electronic properties and field-induced transition from semiconducting to Dirac semimetallic states[26–37]. BP's high carrier mobility[17–21,23] and widely tunable bandgap achieved by controlling the layer number[24,34,38] and external field[35,39] make it promising for various electronic and photonic applications. Interestingly, BP's isoelectronic group IV monochalcogenides in their monolayer form (MX, M = Sn or Ge and X = Se or S)[40–48] have also attracted much attention. The crystalline structure of the monolayer MX is analogous to that of BP but with the broken inversion symmetry, owing to its compound nature. As a result, monolayer group IV monochalcogenides are ideal candidates for the exploration of exotic polarization properties and applications in piezoelectronics and ferroelectronics.

In this forward-looking Review, we first cover various crystalline symmetries and material properties of BP and its isoelectronic group IV monochalcogenides. We also briefly discuss other layered elemental and compound group V materials[49–54]. We then focus on material stability issues and wafer-scale synthesis approaches of BP and MX, which are of particular significance for the future of this group of materials. Subsequently, we cover the new electronic and photonic device concepts and potential pathways for the discoveries of novel physical phenomena, leveraging various exciting properties of this group of materials with diverse crystalline symmetries. Finally, we share our views on future research directions.

Symmetries and basic material properties

The diverse physical properties of BP and its isoelectronic group IV monochalcogenides arise primarily from their material compositions and crystalline symmetries, with breaking and reduction of symmetries playing an important role. In BP, the puckered lattice has only two-fold rotational symmetry, which is much reduced when compared with the six-fold in-plane rotational symmetry in monolayer graphene with a flat hexagonal lattice, as illustrated in BOX 1. As a result, BP's band structure is anisotropic regardless of its thickness, resulting in anisotropic in-plane transport, thermal and optical properties[2,18,19,23]. For example, in monolayer and few-layer BP, the photoluminescence emission is perfectly linearly polarized[24,27,34]. BP also exhibits interesting electrochemical properties, which are sensitive to its environment[55,56]. Its work function highly depends on the layer number, and the redox activity is very different for the basal and edge planes[55]. A few previous reviews[55,57–60] cover in detail the physical properties of BP. We summarize its most basic features below.

Compared with layered semiconducting transition metal dichalcogenides (TMDs), such as molybdenum disulfide (MoS_2)[8], in BP, the layer-to-layer interaction is stronger, leading to a stronger thickness dependence of its bandgap. The electronic bandgap of BP varies from around 0.33 eV to 2.0 eV, when its thickness is reduced from more than ten layers to a monolayer[24]. In bulk BP, the electron (hole) effective masses along the *x*-direction (armchair), *y*-direction (zigzag) and *z*-direction (perpendicular to the 2D plane) were experimentally measured to be around 0.08 (0.08), 1.00 (0.65) and 0.13 (0.28) m_0, respectively, where m_0 is the free electron mass[61]. In few-layer (3–5 layers) BP, electrons and holes were

[1]*Department of Electrical Engineering, Yale University, New Haven, CT, USA.*

[2]*Ming Hsieh Department of Electrical Engineering, University of Southern California, Los Angeles, CA, USA.*

[3]*Department of Electrical and Computer Engineering, Lehigh University, Bethlehem, PA, USA.*

[4]*Centre for Advanced 2D Materials and Graphene Research Centre, National University of Singapore, Singapore, Singapore.*

[5]*Department of Physics, National University of Singapore, Singapore, Singapore.*

[6]*Department of Physics, Washington University, St. Louis, MO, USA.*

**e-mail: fengnian.xia@yale.edu; han.wang.4@usc.edu; lyang@physics.wustl.edu*

https://doi.org/10.1038/s42254-019-0043-5

Key points

- The crystalline symmetries of layered black phosphorus and its isoelectronic group IV monochalcogenides play a very important role in the determination of their physical properties.
- Black phosphorus is likely to be the layered semiconductor material with the highest carrier mobility at room temperature, making it promising for high-performance electronic applications.
- Black phosphorus, arsenic phosphorus and other group V alloys may find applications in mid-infrared photonics as alternative material systems owing to their layered nature and moderate bandgap.
- Monolayer group IV monochalcogenides have a broken inversion symmetry and spontaneous in-plane electric polarization. They present a great platform for the exploration of piezoelectricity, ferroelectricity, ferroelasticity and multiferroics.
- In black phosphorus and other group V alloys, the interplay between the crystal symmetry and spin–orbit coupling may lead to the realization of rich topological states.
- Wafer-scale synthesis of this group of materials remains challenging. Future research may leverage the phase transition induced by pressure, temperature or high-intensity light.

predicted to have similar effective masses of around 0.15 and 1.00 m_0 along the *x*-direction and *y*-direction, respectively[23]. However, the intrinsic properties of monolayer and bilayer BP, including the carrier mobilities, remain unclear[23,62]. Future experiments are required to accurately determine the effective masses and intrinsic mobilities of electrons and holes in monolayer to five-layer BP. Compared with other semiconducting layered TMDs such as MoS_2, high-quality thin-film BP (4 nm and thicker) exhibits much higher carrier mobility. Most notably, ultrathin, high-quality BP (~4 nm thick; 6–8 layers) sandwiched between hexagonal boron nitride (hBN) layers shows an impressive hole mobility of around 5,000 $cm^2\ V^{-1}\ s^{-1}$ at room temperature[63], making it suitable for advanced electronic applications, as discussed in detail in the electronic properties section.

For photonics, the direct, moderate bandgap (~0.33 eV) of thin-film BP enables its strong interaction with light in a broad wavelength range including the technically challenging near-IR and mid-IR[19,29,30] ranges. Moreover, arsenic can be introduced to BP to form an alloy, arsenic phosphorus (As_xP_{1-x}), whose bandgap can be tuned continuously from around 0.33 eV ($x = 0.00$) to 0.17 eV ($x = 0.83$)[54]. Interestingly, BP can be thinned down using plasma without significant degradation in electronic or photonic properties[64].

BP's isoelectronic group IV monochalcogenides in bulk form have previously been explored for various applications. For example, bulk SnSe has been shown to have a high figure of merit for thermo-electronics[65] owing to its unique combination of high electrical conductivity and low thermal conductivity. Both SnS and GeS have been evaluated for photovoltaics because the bandgap of each is around 1.2 eV (REFS[66,67]), close to the optimal bandgap of 1.3 eV for single-junction solar cells. In this Review, we focus on monolayer monochalcogenides with low C_{2v} crystalline symmetry, in which the inversion symmetry is further broken as shown in BOX 1. This makes it possible to observe new order parameters and polarization properties. Giant piezoelectricity, ferroelectricity and even multiferroics of ferroelectricity and ferroelasticity are expected in monolayers[43,44,46,47].

Box 1 | Symmetry group of monolayer graphene, pnictogens and monochalcogenides

New physics is usually associated with symmetry breaking. The parent isotropic structure, graphene, has the highest symmetry (D_{6h}), which has a six-fold in-plane rotation, six two-fold perpendicular axes and a horizontal mirror plane (top left). The buckling structure of arsenene and antimonene (bottom left) reduces the D_{6h} symmetry to that of D_{3d}, which contains a three-fold rotation, three two-fold perpendicular axes and three mirror planes, resulting in their rather isotropic in-plane properties. The puckered structure of monolayer black phosphorus (BP; top right) reduces the D_{6h} symmetry of graphene to that of D_{2h}, which contains a two-fold rotation, two two-fold perpendicular axes and a mirror plane, leading to highly anisotropy electronic, thermal and optical properties. The further lower-symmetry structure (C_{2v}), which only contains a two-fold rotation and two mirror planes, can be obtained from D_{2h} by breaking the inversion symmetry in bi-element group IV monochalcogenides (bottom right), making them ideal for the exploration of electric polarization properties. Other than these intrinsic symmetries, extrinsic factors, such as strain, external electric fields and alloying, can tune these symmetries and corresponding physical properties and enable device applications.

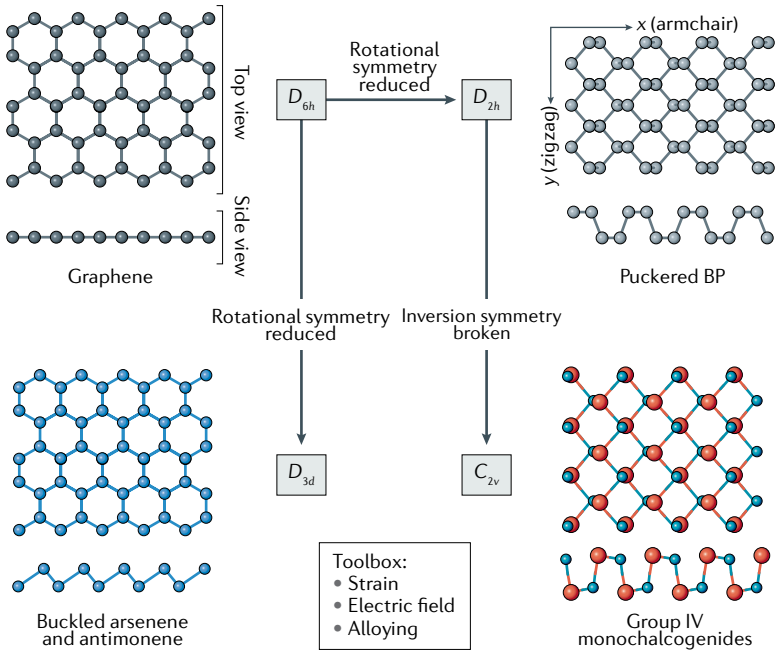

Puckered group V (BP, arsenic phosphorus and possible antimony phosphorus, as discussed below) and group IV–VI materials all belong to an orthorhombic crystal system and are all semiconductors. Our main motivation to review them together is to illustrate how the crystal symmetry and spin–orbit coupling (SOC) play critical roles in the determination of their physical properties. We focus on their interesting physical properties and the most likely applications in photonics and electronics. For BP, we concentrate on its thin-film form in mid-IR photonics and its few-layer form in electronics. For group V alloys, we focus on their tunable topological properties enabled by the strong SOC. For group IV–VI monolayers, we emphasize their interesting physical properties due to the intrinsic broken inversion symmetry.

The heavier group V materials, such as bulk arsenic, antimony and bismuth, assume a buckled honeycomb structure and are all metallic[51–53]. As shown in BOX 1, buckled free-standing monolayer arsenic (arsenene), antimony (antimonene) and bismuth (bismuthene) are predicted to be stable and semiconducting[49–53], although recent theoretical studies show that puckered free-standing monolayer arsenic and antimony can also be thermodynamically metastable[68]. Buckled monolayers have three-fold rotational symmetry, as illustrated in BOX 1, and their band structures and phonon energy dispersions are more isotropic than those of monolayer BP[69]. Moreover, the stronger SOC is predicted to enhance the hole mobility in monolayer arsenic and antimony owing to SOC-induced valence band splitting and modification of the hole effective mass[69]. Extensive theoretical investigations and preliminary experimental results have illustrated their interesting properties, ranging from topological properties[70] to the metal semiconductor transition made by varying the layer number and external strain,[49–53,68]. These layered group V materials are very interesting materials and deserve further exploration. However, in this Review, we do not cover them in detail owing to space limitations.

External electric field, doping, pressure and strain can further significantly modify the physical properties of these materials. The physical properties of few-layer and thin-film BP are widely tunable by doping[28], vertical electric field[35,39,71–74] or pressure[75,76], which enable tunable electronic and optical responses, as well as the observation of band inversion, topological insulators and nodal line semimetals. Interestingly, the puckered structure of BP and group IV monochalcogenides leads to a profound effect of external strain that affects the lattice spacing and material properties[22,43,77].

Material stability and synthesis

Stability. To produce new devices using emerging materials, one should first demonstrate long-term stability of the device. One major concern in the 2D material and device community is that BP and its related materials are, in general, unstable in air. Indeed, as other widely used materials such as silicon and germanium, BP can react with oxygen[78], forming phosphorus oxide on its surface. Photons can accelerate the oxidation effect in BP, and water vapour can further transform the phosphorus oxide into aqueous phosphoric acid, making naked BP devices unstable in air[79]. Detailed degradation processes of AsP devices have not been reported, and they are likely to behave similarly to BP devices. To date, many effective surface passivation schemes have been demonstrated to dramatically improve BP device stability. It was shown that BP encapsulated by aluminium oxide (AlO_x) deposited using atomic layer deposition has long-term stability even in air[80]. Without encapsulation, the BP surface developed bubbles quickly, whereas the encapsulated BP remained smooth in the long term. FIGURE 1a denotes the atomic force microscopy image of the BP surface without AlO_x (left) and with AlO_x (right). Moreover, the long-term stability of monolayer and few-layer BP sandwiched between hBN layers in ambient conditions, even under strong laser irradiation, was demonstrated elsewhere[81]. Other than hBN and atomic-layer-deposited oxide, covering BP with self-aligned molecules[82] also prevents degradation and leads to long-term device stability. In FIG. 1b, the long-term stability of the BP transistor encapsulated in aluminium oxide is illustrated, as in a previous study[83], in which the transistor's transfer characteristics did not degrade for over 7 months. Interestingly, even without an encapsulation monolayer, SnSe shows much better long-term stability in ambient conditions than BP does, owing to its stronger bonds[84]. This observation is consistent with the theoretical prediction in a previous study[45]. The various scalable encapsulation schemes have demonstrated long-term effectiveness and can be leveraged for future development of devices. In addition, different types of defects in BP are predicted to have different stabilities, and they can strongly affect BP's physical properties[85,86]. As a result, defects could play an important role in the degradation of BP, which suggests that improving the quality of BP may further enhance its long-term stability.

Synthesis. To date, most reported BP and AsP devices are based on few layers or thin films mechanically exfoliated from bulk crystals. Bulk BP was first obtained by converting red or white phosphorus under high pressure and high temperature[1]. Recently, catalyst-based synthesis in ampoules successfully resulted in millimetre-scale BP and AsP clusters[87,88], from which high-quality thin films can be exfoliated. By contrast, there are few reports on wafer-scale synthesis of BP. Red phosphorus thin film was converted into BP in some isolated areas under a pressure of 2.7 MPa at 950 °C with mineralizing agents[89]. Under a pressure of 8 GPa, 10–40 nm-thick red phosphorus was successfully converted into nanocrystalline BP at room temperature on a 4 mm diameter flexible substrate [90]. Using pulsed laser deposition, wafer-scale amorphous BP as thin as 2 nm was produced[91]. However, in both wafer-scale cases, the quality of the BP was inferior to that of exfoliated BP. BP has also been chemically exfoliated and stabilized in solvent[92]. Although the quality of chemically exfoliated BP can be high, this approach cannot readily produce wafer-scale continuous thin films.

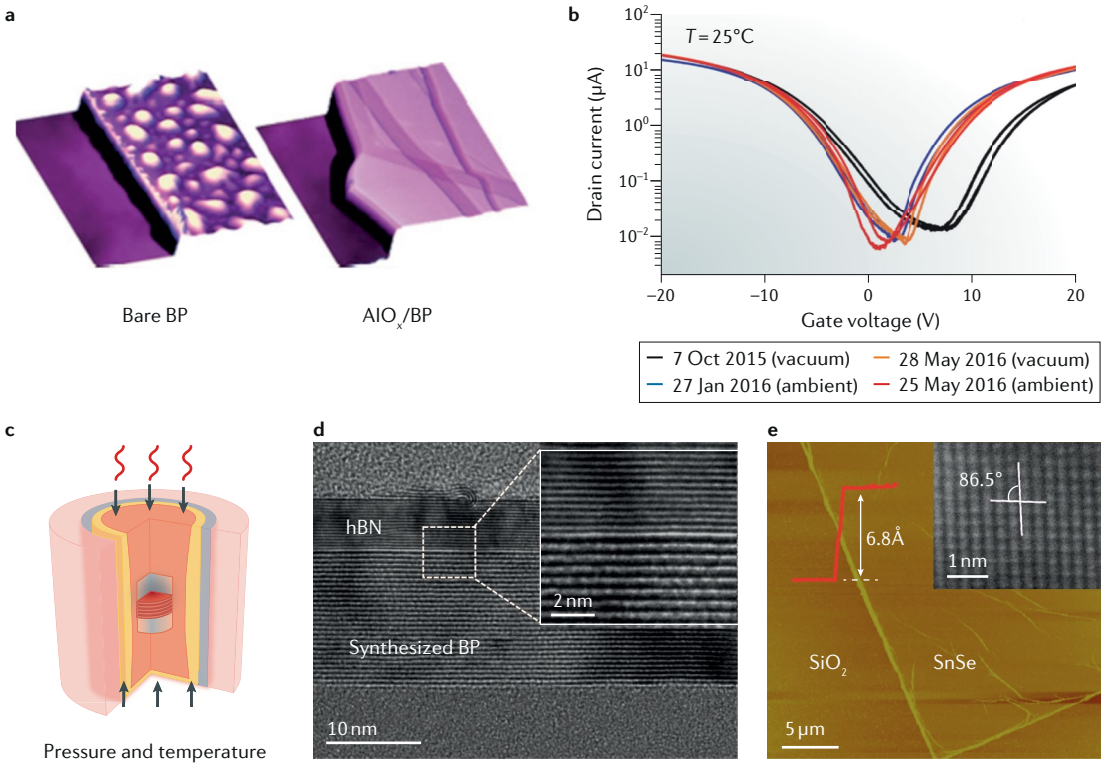

Fig. 1 | **Synthesis and stability of black phosphorus and monolayer SnSe. a** | Atomic force microscopy (AFM) images of black phosphorus (BP) exposed to air without AlO_x (left) and with AlO_x (right) encapsulation. The images are 3D plots of the original AFM images, which have a size of 6.2 × 6.2 μm with a z-axis of [0,200] nm for the left image and 6.3 × 6.3 μm with a z-axis of [0,106] nm for the right image. **b** | Transfer characteristics of BP transistors encapsulated within Al_2O_3, demonstrating long-term stability. **c** | Wafer-scale red phosphorus partially covered by hexagonal boron nitride (hBN) flake converted into BP under high pressure and high temperature. **d** | High-resolution transmission electron micrograph of converted BP. Inset presents an enlarged view of the atomically sharp hBN–BP interface. **e** | Atomic force micrograph of synthesized monolayer SnSe. Inset presents a high-resolution transmission electron micrograph. Panel **a** is reproduced with permission from REF.[80], ACS. Panel **b** is reproduced with permission from REF.[83], ACS. Panels **c** and **d** are reproduced with permission from REF.[93], Wiley-VCH. Panel **c** was designed by C. Li, Yale University, USA. Panel **e** is reproduced with permission from REF.[84], IOP.

Most recently, red phosphorous thin films on 5 mm diameter sapphire substrates were successfully converted into BP at 1.5 GPa and 700 °C (REF.[93]). In this approach, red phosphorous was first deposited by physical vapour deposition on the sapphire substrate, and an exfoliated few-layer hBN flake was transferred on top of the red phosphorous. In subsequent conversion at elevated pressure and temperature, as shown in FIG. 1c, phosphorus atoms become mobile and form highly crystalline BP with domain size on the order of tens of micrometres, as confirmed by Raman and IR extinction spectroscopy[93]. More importantly, by partially covering the red phosphorus with few-layer hBN before conversion, a nearly perfect hBN–BP interface was achieved after conversion, as shown in FIG. 1d.

The estimated minimum pressure for the conversion from red phosphorus into BP can be around 200 MPa (REF.[94]), and recently, the successful conversion of red phosphorus into BP at 400 MPa (REF.[95]) implies that this conversion approach may be applied to red-phosphorus-covered wafers well beyond the inch scale. Another major advantage of this approach is that multiple wafers can be stacked and processed together with high throughput. Moreover, such pressure-induced phase transitions may also be applied to synthesize wafer-scale AsP. Since wafer-scale few-layer hBN synthesis and transfer have been demonstrated successfully[96], this approach lays the foundation for future realization of hBN–BP (or hBN–AsP) heterostructures at wafer scale, which are ideal for advanced electronic and photonic applications. Other than the pressure-induced phase transition, molecular beam epitaxy (MBE) is another promising route towards large-scale synthesis. Monolayer blue phosphorus, another phosphorus allotrope, has been successfully grown on a gold (111) surface[97] using MBE. Few-layer BP may be grown using MBE if appropriate substrates can be identified, because the substrate can play a critical role in the epitaxial growth of BP[98].

Various high-quality MX monochalcogenides have been synthesized in the bulk form. For example, the vapour transport growth of thin-film SnSe from high-purity SnSe powder was demonstrated[99]. In this case, thin-film SnSe as thin as ~6 nm was produced. However, although other high-quality thin-film MXs can be similarly grown by vapour transport growth, their thicknesses tend to be above 5 nm (~10 layers). This is most likely due to their strong layer-to-layer interaction[100], which promotes vertical growth and also

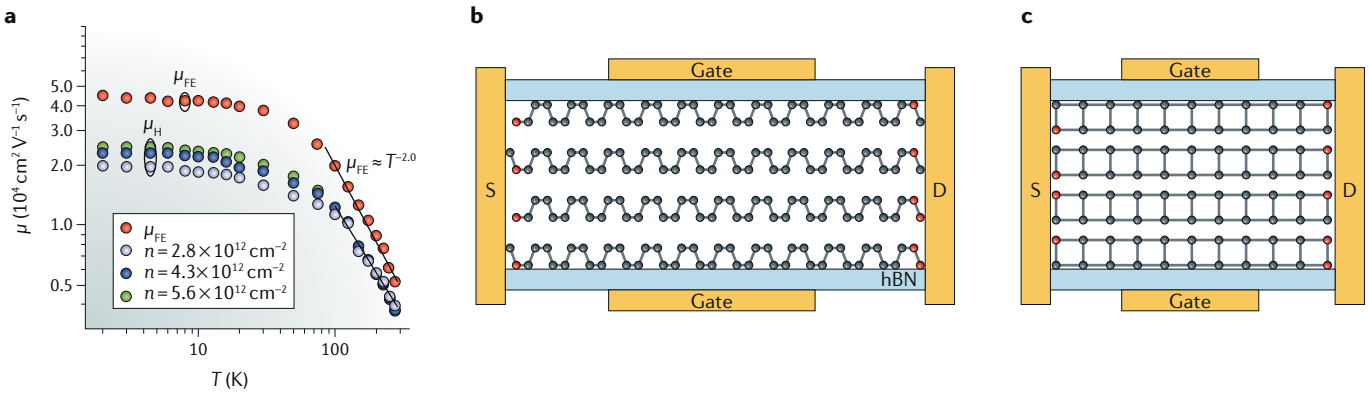

Fig. 2 | **Few-layer black phosphorus transistors. a** | Field effect (μ_{FE}) and Hall (μ_H) mobilities measured along the armchair direction of ~4 nm-thick black phosphorus (BP) exfoliated in vacuum. **b** | Schematic of a BP transistor with its channel aligned in the armchair direction for high speed. **c** | Schematic of a BP transistor with its channel aligned in the zigzag direction for minimal source (S)–drain (D) tunnelling when the channel is shorter than 5 nm. The red atoms indicate dopants for minimal contact resistance. hBN, hexagonal boron nitride; *n*, carrier density. Panel **a** is reproduced with permission from REF.[63], ACS.

makes mechanical exfoliation of few-layer MX challenging. Although 1 nm-thin SnSe films have been produced chemically on a submicrometre scale using one-pot synthesis in the presence of oleylamine and phenanthroline[101], this approach cannot be used to produce continuous few-layer MXs on a wafer scale. The suppression of vertical growth is hence critical for the future direct synthesis of large-scale monolayer and few-layer MXs. An alternative two-step method for the synthesis of large-area monolayer SnSe was demonstrated, which may also be applied to the synthesis of other monochalcogenides[84]. In this approach, a tens-of-nanometers thin film of SnSe was first grown and then thermally etched at 700 °C in a nitrogen or argon/hydrogen environment. Thus, large-area monolayers of SnSe on a tens-of-micrometres scale were realized in which the etching process is self-limiting when the film reaches the monolayer thickness, as shown in FIG. 1e, probably owing to the strong interaction between the SnSe and the silicon dioxide substrate. The high-resolution transmission electron microscopy image indicates that such monolayer SnSe is highly crystalline, as shown in the inset of FIG. 1e. Although the detailed etching mechanism requires further investigation, this work represents the first demonstration of the large-scale synthesis of monolayer SnSe. A future detailed characterization may reveal the exciting properties of monolayer SnSe. In addition, MBE can be another promising direction for the growth of monolayer and few-layer MXs. Other than four MXs discussed above, monolayer SnTe, a material close to orthorhombic MX discussed in this Review, has been grown on graphene by MBE with interesting in-plane ferroelectricity[102]. Very likely, other monolayer MXs can also be grown using MBE in a similar manner with the proper choice of substrate.

Electronic properties of BP

Layered BP is a thin-film (below 10 nm) semiconductor in which the mobilities of both electrons and holes are high at room temperature, ideal for advanced electronic circuits[103,104]. Numerous high-mobility BP transistors have been reported since 2014. In a previous study[17], the hole effective mobility in an ~10 nm-thick BP was measured to be around 1,000 cm^2 V^{-1} s^{-1}. In fact, the semiconductor industry has been exploring various high-mobility materials beyond silicon for decades, with III–V compound semiconductors[105] and germanium[106] being the leading candidates. Compared with these 3D materials, the layered nature of BP allows for the realization of high-mobility transistors with ultrathin channels without dangling bonds on the surface, which is advantageous for transistor scaling with excellent electrostatic control. In an ~4 nm-thick (6–8 layers) BP sandwiched between hBN layers, fieldeffect hole mobility as high as 5,000 cm^2 V^{-1} s^{-1} along the armchair direction was reported at room temperature[63], as shown in FIG. 2a. The field effect mobility (μ_{FE}) and the Hall mobility at different doping concentrations (μ_H) both exhibit a temperature dependence close to T^{-2} at high temperature, indicating that the scatterings are mainly with phonons and that the BP material is close to be intrinsic. Furthermore, at low temperature, the carrier mobility is greater than 2×10^4 cm^2 V^{-1} s^{-1} even at hole doping above 3×10^{12} cm^{-2}. Moreover, adatom-doped BP transistors have high field effect electron mobility, reaching 380 cm^2 V^{-1} s^{-1} in 10 nm-thick BP at room temperature[107] and 1,495 cm^2 V^{-1} s^{-1} in 5 nm-thick BP at 260 K (REF.[108]) with copper and aluminium adatoms, respectively. These encouraging results further reveal the potential of BP in high-speed and high-frequency electronics. To underscore the potential of BP for advanced electronics, cut-off frequencies in the microwave range have been shown for BP transistors fabricated on both high-resistivity silicon and flexible plastic substrates[103,104,109,110].

For transistors with a relatively long channel whose length is greater than the carrier mean free path, mobility plays a decisive role in their performance. High carrier mobility leads to an improved ON state current and reduced carrier transit time. However, for ultrashort channel transistors (5 nm and below), the transport can be close to being ballistic with negligible scattering in the channel. Under high source–drain bias, carrier saturation

velocity determines the transit time. Indeed, in this case, mobility is no longer an accurate metric to gauge transistor performance. However, carrier mobility still plays an important role, even in ballistic transistors. First, the carrier injection efficiency from source to drain can be affected by mobility. Even in short-channel length ballistic transistors, high mobility is still desirable to reduce backscattering for carriers injected from the source to the channel, as pointed out elsewhere[111]. Second, in high-mobility material, a lower critical field is needed for velocity saturation[112,113]. As a result, it is possible to use a smaller source–drain bias for saturated operation, leading to reduced power consumption. Lastly, high mobility is critical to the reduction of parasitic resistances such as contact and access resistance. In short, the industry has been looking for high-mobility semiconductors for decades, and BP seems to be a promising candidate.

Advanced electronic circuits can be made from BP transistors only if they are viable to form hBN–BP–hBN heterostructures or to replace hBN with other high-quality dielectrics on a wafer scale. As discussed above, the recent successful conversion of hBN-covered red phosphorus into BP lays a solid foundation for the future realization of such high-quality, air-stable hBN–BP–hBN heterostructures on a wafer scale. As the carrier mobility may be low in monolayer and bilayer BP owing to its low-pair of out-of-plane *p* electrons[62], for advanced electronics, the community probably needs to focus on few-layer BP (4–8 layers), in which high mobility has already been shown experimentally[63,81].

For high-performance BP transistors, high-quality gate dielectric and low-contact resistance are two other key ingredients. FIGURE 2b shows a conceptual long-channel transistor in which the few-layer BP (along the high-mobility armchair direction for high speed) is sandwiched between thin-film hBN layers. In this case, hBN is used as both high-quality gate dielectric and surface passivation, as first demonstrated on graphene in a previous study[114]. Moreover, it may be possible to leverage the traditional ion implantation and dopant activation techniques to selectively dope BP near edge contacts[115], with hBN protecting the BP from damage during implantation and activation.

For a transistor channel length shorter than 5 nm, source–drain direct tunnelling can lead to significant leakage[116]. To suppress tunnelling, large carrier effective mass becomes desirable[116,117], and one can take advantage of the high anisotropy of BP. Along the zigzag direction, few-layer BP has a large effective mass ($\sim m_0$) for both electrons and holes, where m_0 is the free electron mass. Therefore, an ultrashort channel can be built along the zigzag direction to suppress source–drain tunneling, as shown in FIG. 2c. Despite the large effective mass, the mobility of few-layer BP along the zigzag direction is still impressive[2]. Another requirement for deeply scaled transistors is that the BP thickness should be much smaller than the transistor channel length. For ultrathin few-layer BP with a thickness in the range of 2–4 nm (~4–8 layers), the calculated electronic bandgap is in the range of 0.7–0.4 eV (REF.[24]), which is larger than the bulk BP bandgap and is desirable for the suppression of the OFF state current.

Finally, another particularly promising direction is to monolithically integrate ultrathin BP with silicon or III–V compounds[105] to enhance the p-type transistor performance, leveraging the high hole mobility in BP. Previously, germanium has been explored for this purpose[106]. However, growth of ultrathin high-quality germanium on foreign substrates is very challenging. Integration of ultrathin BP with silicon or III–V compounds may significantly boost the performance of complementary logic circuits.

Optical properties of BP and AsP

Photonic materials covering a broad wavelength range in mid-IR and suitable for monolithic integration are very desirable[118]. Previously, various BP IR photodetectors have been used, and their unique capability to resolve incident light polarization owing to BP anisotropy can be extremely useful[29,119]. However, the cut-off wavelength of BP photodetectors relying on the interband transition is around 3.7 μm, corresponding to a bandgap of around 0.33 eV. In AsP, the bandgap can be continuously tuned from 0.33 eV to around 0.17 eV by varying the arsenic mole fraction from 0% to 83%[54], extending the coverage to longer wavelengths[120,121]. For example, a previous study[120] reported the detection of mid-IR light up to 8.05 μm using an $As_{0.83}P_{0.17}$ photodetector, as illustrated in FIG. 3a. The I–V characteristics shown in FIG. 3a with (red) and without (black) 8.05 μm light excitation vary significantly, indicating the generation of bias-dependent photocurrent (blue). Moreover, the vertical electric field applied to few-layer and thin-film BP was shown to dynamically tune its bandgap[35,39]. The study[35] showed that this bandgap tuning strongly depends on the BP thickness owing to the competition between interlayer interaction and the overall potential drop. As illustrated in FIG. 3b, a moderate field of around 1 V nm^{-1} can tune the bandgap of ~10 nm-thick BP from its pristine value of ~0.33 eV to below 0.1 eV (red dots), further extending the coverage beyond that of AsP without an electric field. Moreover, the observed bandgap tuning results (red dots) are much smaller than those obtained from simple tight-binding calculations (red dashed line)[35]. However, after the variation of the BP dielectric constant as a function of the bandgap has been taken into account, the calculated bandgap tuning results (solid red line) agree with the measured results (red dots) very well, as shown in FIG. 3b (also shown elsewhere[35]). Here, the bandgap tuning (~0.2 eV) is significant when compared with that of the pristine BP bandgap (~0.33 eV). This is very different from the traditional quantum-confined Stark effect in III–V quantum wells, in which the tuning of the energies of the confined carriers is much smaller than the bandgap itself, and the Stark effect is approximately quadratic[122]. The widely tunable bandgap in BP and AsP, together with their intrinsic layered nature, makes them particularly promising in the realization of integrated mid-IR photonic circuits.

Looking forward, thin-film BP and AsP can play important roles in waveguide-integrated mid-IR photonic circuits for sensing and communication applications. Their thin-film nature makes them ideal for monolithic integration. Moreover, stronger light–matter

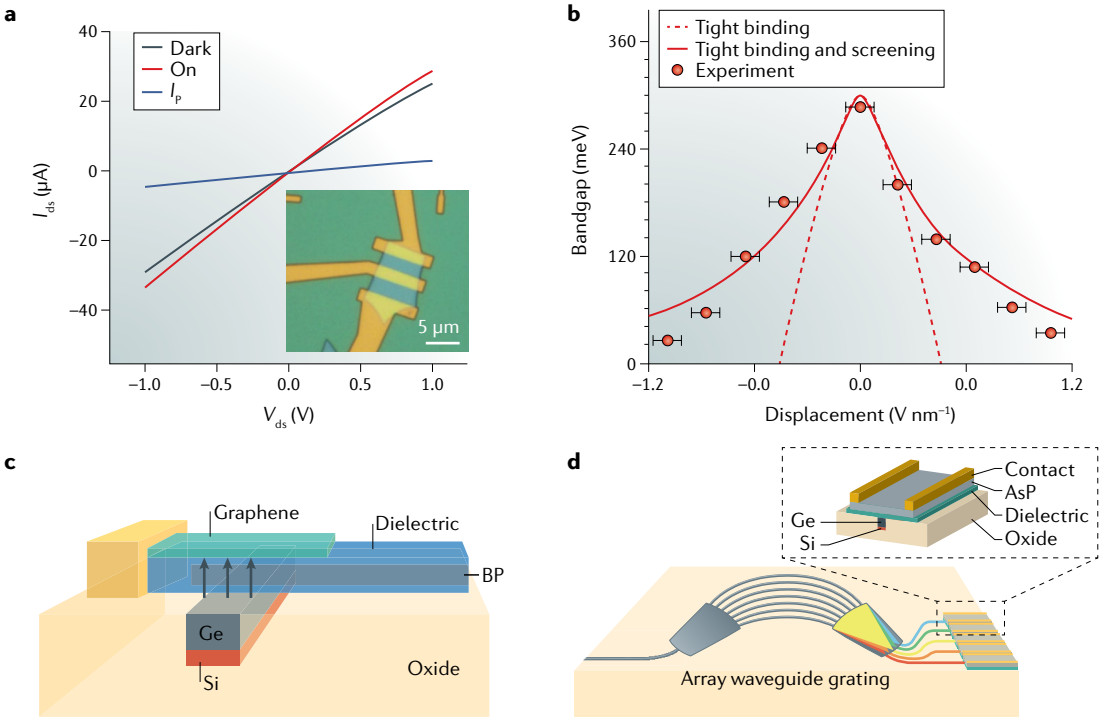

Fig. 3 | **Black phosphorus and AsP photonics. a** | Mid-IR detection at 8.05 μm by AsP. Inset depicts a micrograph of an AsP photodetector. **b** | Bandgap tuning of ~10 nm-thick black phosphorus (BP) by a vertical electric field. **c** | A BP mid-IR modulator integrated with a germanium waveguide. The electric field is applied through the top graphene and the bottom germanium (grey arrows). **d** | An on-chip mid-IR spectrometer integrating an array waveguide grating with an AsP mid-IR detector array. I_{ds}, source–drain current; I_p, photocurrent, which is the difference in I_{ds} between the light on and dark states; V_{ds}, source–drain bias voltage. Panel **a** is reproduced with permission from REF.[120], AAAS. Panel **b** is reproduced from REF.[35], CC-BY-4.0. Panels **c** and **d** were designed by X. Yan, University of Southern California, USA.

interaction can be achieved through integration with passive optical structures, reducing the amount of active material needed. As a result, these integrated mid-IR devices can have a low dark current. For example, FIG. 3c shows a schematic of a proposed mid-IR BP waveguide modulator, in which mid-IR light is guided by low-loss germanium on a silicon-on-insulator. In this case, silicon is used as the seeding layer for thick germanium growth[123]. It is also possible to use other materials such as chalcogenide glass[124] or suspended germanium[125] for mid-IR waveguiding. The thin-film (~10 nm) BP is sandwiched between two dielectric layers, and a vertical electric field can be applied through the bottom germanium and the top transparent electrode (for example, graphene). Recently, waveguide-integrated mid-IR BP photodetectors operational within 2–4 μm have been demonstrated[126,127]. In the optical modulator proposed in FIG. 3c, the electric field can tune the BP bandgap from around 0.33 eV to below 0.1 eV (REF.[35]), covering a wavelength range of approximately 4–12 μm. Such modulators can have at least a gigahertz bandwidth. The device structure in FIG. 3c is different from a previously proposed BP waveguide modulator[73], in which one electrode is in direct contact with BP and the Pauli-blocked Burstein–Moss effect can blue-shift the absorption edge[71,74]. Moreover, it is even feasible to construct on-chip mid-IR spectrometers, as shown in FIG. 3d. In such a spectrometer, broadband mid-IR light is first coupled to the input waveguide, then spectrally separated into different waveguides using a mid-IR array waveguide grating[128] and finally detected by an As_xP_{1-x} (or electrically tuned BP) photodetector array. Such an on-chip mid-IR spectrometer can find applications in gas sensing and multispectral surveillance systems. In modulators and spectrometers, the armchair crystal orientation of BP and AsP should be aligned with light polarization to maximize the light–matter interaction. Other than mid-IR light modulation and detection, with further improved crystal quality, mid-IR light-emitting diodes or even lasers may be realized on the basis of hBN–BP–hBN heterostructures.

Moreover, AsP with high arsenic concentration may be used to construct mid-IR imagers. Although in mid-IR, mercury cadmium telluride (HgCdTe) imagers show high efficiency with low dark current and have been commercialized for decades, the industry is seeking to replace HgCdTe owing to various materials issues such as non-uniformity, instability and difficulty to scale up and integrate with silicon readout circuits[129]. Wafer-scale encapsulated thin-film AsP is a promising alternative material for mid-IR imagers, which in principle can be compatible with arbitrary substrates.

Finally, for photonic applications, the optimal thickness for BP and AsP should be greater than 10 nm for strong light–matter interaction in mid-IR. As a result, the requirements for synthesis are much less demanding. Most likely, BP and AsP will find applications in photonics before electronics.

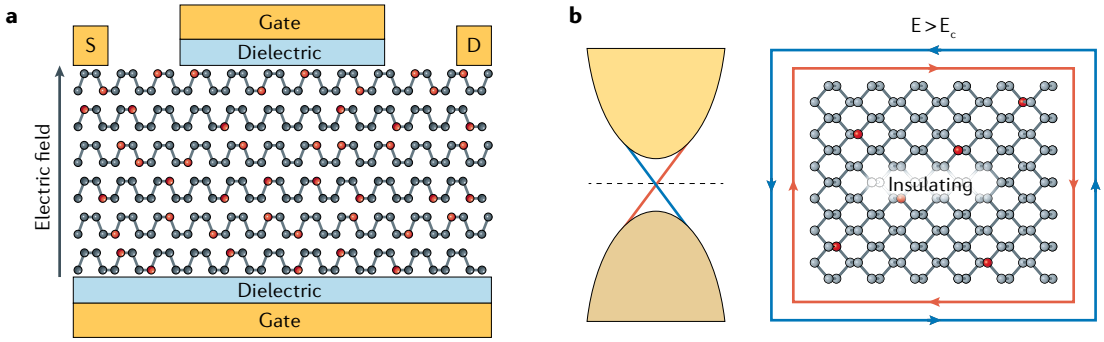

Fig. 4 | **Tunable topological insulating properties. a** | Schematic of a dual-gate AsP 2D topological transistor. The grey arrow represents the vertical electric field. **b** | Schematic band structure and insulating channel when the biasing field (E) is larger than the critical field needed for band inversion (E_C). The red and blue arrows represent spin-up and spin-down currents, respectively. Red and grey spheres represent As and P atoms, respectively. D, drain; S, source. Panels **a** and **b** are adapted with permission from REF.[37], ACS.

Topological properties of group V materials

SOC is important for BP and group V compounds. In particular, the interplay between SOC and crystal symmetry can lead to many interesting physical phenomena, including the realization of rich topological states. For few-layer BP, a band inversion can be achieved by the gating field. Then, SOC can generate a finite bandgap, making gated few-layer BP a 2D topological insulator (TI)[37]. The estimated critical field for realizing a tunable TI in four-layer BP is as large as 3 V nm^{-1}, which makes experimental implementation challenging. Fortunately, the critical field can be reduced by choosing thicker BP, because thicker material can lead to larger bandgap tuning owing to the enhanced potential difference along the direction of the electric field[35].

In the future, AsP or other group V compounds with heavier Sb and Bi with the puckered structure can be leveraged for the realization of tunable TI, because they are expected to have a similar band structure to BP[130] but a smaller intrinsic bandgap[54]. Furthermore, the heavier As, Sb or Bi atoms may contribute to stronger SOC, which can result in a larger bandgap opening of the TI state. FIGURE 4a illustrates such a dual-gated few-layer AsP tunable TI transistor. FIGURE 4b indicates the TI state when the vertical electric field exceeds the critical amplitude.

For bulk BP, a moderate pressure (around 0.6 GPa) can also induce the band inversion[76]. Under pressure, the dimension of the Fermi surface of bulk BP can reduce to a line through a Lifshitz transition, leading to a nodal line semimetal, in which a Dirac cone-like energy dispersion is formed, as observed in compressed BP[75]. This phenomenon arises from the D_{2h} crystal symmetry and the chiral nature of electrons in BP. As a result, the effective Hamiltonian contains the forms of both Dresselhaus and Rashba SOCs[131], although true SOC cannot exist in intrinsic BP because of the inversion symmetry. This analogous SOC term can be regarded as pseudo-SOC. The strength of the pseudo-SOC in BP is 1–2 orders of magnitude larger than that of typical SOC[132]. More possible topological properties of BP and AsP can be realized with different symmetries. For example, 2D symmetry-protected (topological) Dirac semimetallic states have been observed in BP[133].

In the future, the experimental realization of tunable topological materials could be a very promising research direction for few-layer BP and group V compounds. For example, after further consideration of true SOC and breaking of the inversion symmetry in compressed BP, a finite bandgap may be formed in this nodal line semimetal, translating it into a 3D strong TI. Meanwhile, tuning the electronic structure and symmetry by electrical gating, strain or charge transfer induced by metal adatoms will present opportunities for the exploration of various topological properties.

Ordered phase and polarization properties of MX

Beyond BP, monolayer MXs break the inversion symmetry, reducing the point group to C_{2v} and allowing for the occurrence of electric polarization. This electric polarization can be efficiently tuned by external strain or optical excitation, resulting in enhanced piezoelectric[43] or photostrictive[134] effect (a converse piezoelectric effect resulting in the generation of strain by photons). Moreover, new order parameters, such as spontaneous polarization and strain, emerge in monolayer MXs, leading to ferroelectricity and ferroelasticity. Interestingly, these order parameters can coexist in monolayer MXs, giving rise to multiferroics[47,48].

Giant piezoelectricity. Piezoelectric materials can convert mechanical energy into electricity. 2D materials are interesting for piezoelectric devices because of their ability to withstand large strain[135,136]. Many 2D materials have been predicted to be piezoelectric owing to the broken inversion symmetry in monolayer form, such as hBN and several TMDs[137,138]. Recently, the piezoelectric effect has been demonstrated in monolayer and odd-layer MoS_2 (REFS[139,140]). Compared with other 2D piezoelectric materials, in monolayer MXs, the electronic polarization and piezoelectric effect are significantly enhanced because of their ionic polar nature and the significantly smaller elastic stiffness of the puckered structure. A giant piezoelectric effect has been predicted in these monolayers[43]. Their piezoelectric coefficients can be 1–2 orders of magnitude larger than those of other 2D materials, such as MoS_2, and the widely used bulk quartz, zinc oxide and aluminium nitride, as illustrated in FIG. 5a. In fact,

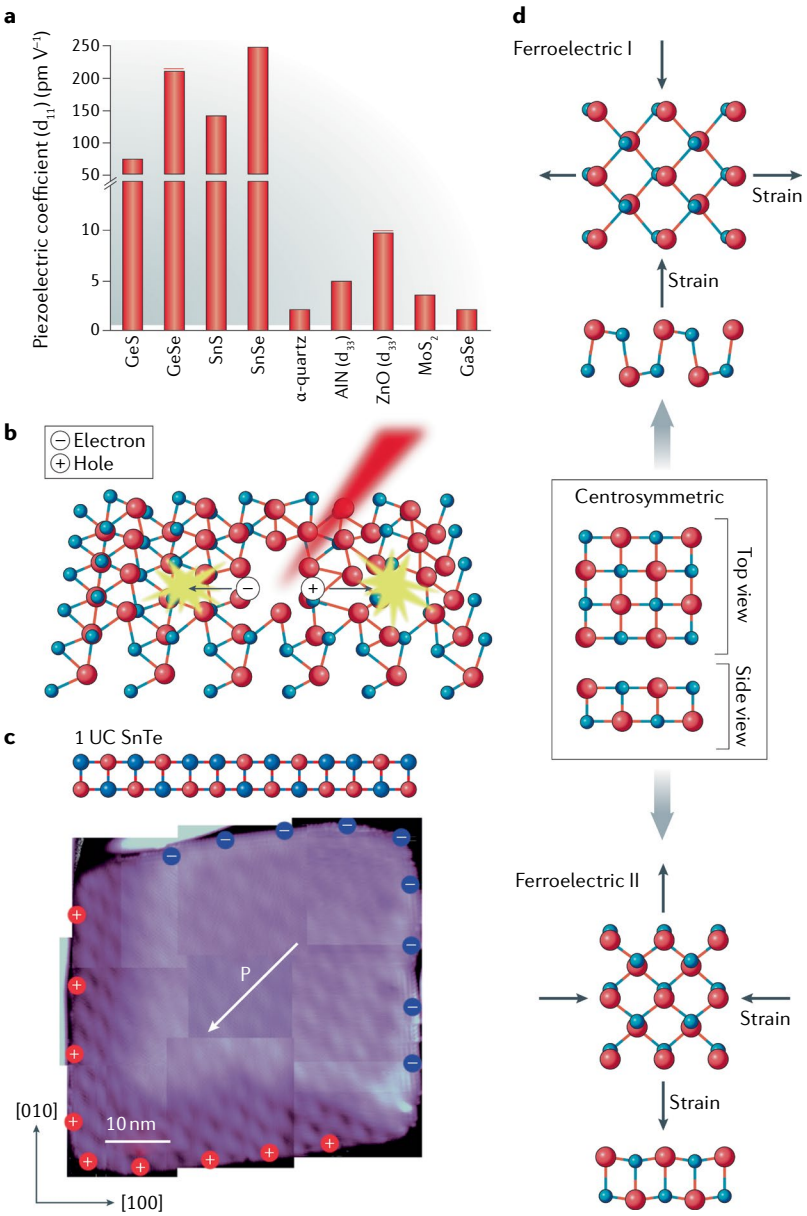

Fig. 5 | **Polarization properties in monolayer MXs. a** | Predicted large piezoelectric coefficients in a typical monolayer MX (M = Ge or Sn; X = S or Se). The piezoelectric coefficients of traditional materials such as quartz and molybdenum disulfide (MoS_2) are also plotted for comparison. **b** | Schematic illustration of the photostrictive effect in monolayer MX, in which light induces lattice strain. The red spheres are the metal atoms (M), and the blue spheres are the chalcogen atoms (X). **c** | The spontaneous in-plane polarization (P) in a ferroelectric monolayer SnTe grown on graphene. The red and blue spheres represent the Sn and Te atoms, respectively. **d** | Multiferroics in monolayer MX. Their centrosymmetric parent phase can relax along both *x* and *y* directions, resulting in two spontaneous lattice strains perpendicular to each other. UC, unit-cell thickness. Panel **a** is reproduced from REF.[43], Fei, R. et al. Giant piezoelectricity of monolayer group IV monochalcogenides: SnSe, SnS, GeSe, and GeS. *Appl. Phys. Lett.* **107**, 173104 (2015), with the permission of AIP Publishing. Panel **c** is reproduced with permission from REF.[102], AAAS.

optically excited electrons and holes can couple with ionic, polar lattices resulting in a photostrictive effect. An enhanced photostrictive effect has been predicted in monolayer MXs[134], as illustrated in FIG. 5b. The structural change is expected to be approximately ten times larger than that observed in perovskites[134].

Given the experimental advances in the synthesis of monolayer MXs[84], the demonstration of this giant piezoelectric effect in MXs can be expected in the near future. This enhanced effect may further be leveraged for a broad range of sensing, piezotronics and energy harvest applications, such as remotely switchable memory devices and light-induced actuators[141,142].

2D ferroelectricity. Beyond strain-induced polarization, a spontaneous in-plane electric polarization has been predicted in MXs[44,47,143]. The amplitude of the spontaneous polarization is comparable to those of the widely used perovskites[44], and the polarization can be switched under a moderate external field[47] (~0.2 V nm^{-1}). Another unique, attractive property of this in-plane 2D ferroelectricity is its relatively high Curie temperature. Contrary to ferromagnetism, in which a lower dimensionality usually weakens the magnetism and reduces the Curie temperature owing to enhanced thermal fluctuations, 2D ferroelectricity is predicted to be robust above room temperature. For example, the Curie temperature of monolayer SnSe calculated by effective Hamiltonian Monte Carlo simulations is around 320 K (REF.[44]). This relatively high transition temperature reflects enhanced Coulombic interaction in 2D structures owing to a reduced screening effect.

A robust in-plane ferroelectricity was observed[102] in monolayer tin telluride (SnTe), a material closely related to orthorhombic MXs. As shown in the top panel of FIG. 5c, intrinsic SnTe has a centrosymmetric rock-salt structure. However, for atomic-thick samples grown on a graphene–silicon carbide substrate, a cubic-to-rhombohedral structural phase transition was observed, resulting in in-plane spontaneous polarization as illustrated on the bottom of FIG. 5c (also shown elsewhere[102]). In the future, advances in the synthesis of MXs, as discussed above, may enable the observation of similar in-plane, room temperature ferroelectricity in monolayer MXs. This ferroelectricity is expected to be robust even around room temperature[44] and may be leveraged to build nonvolatile ferroelectric random-access memory devices.

Beyond ferroelectricity, the ferroelastic effect has been predicted in monolayer MXs[47,48,143]. As shown in FIG. 5d, the centrosymmetric square lattice (the rock-salt structure) of monolayer MXs can undergo a spontaneous relaxation along the *x* or *y* direction, leading to two different orthogonal orientations of the rectangle lattice structures and lattice strain — the ferroelastic effect[48,143]. Combined with the ferroelectric effect, this ferroelastic effect makes monolayer MXs multiferroic. Moreover, because both ferroelasticity and ferroelectricity result from the broken inversion symmetry, the coupling between electrical polarization and ferroelastic strain will be significant. Therefore, given the potentially high Curie temperature of ferroelectricity in these 2D MXs, multiferroics are expected to be stable above room temperature, making monolayer MXs promising for shape and nonvolatile memories[144] and optical devices with enhanced second harmonic generation[145].

MXs have polarization properties similar to those of known bulk ferroic and multiferroic materials, such as perovskite oxides. For example, the piezoelectric

coefficient of $BaTiO_3$ is about 200 pm V^{-1} (REF.[146]) and its spontaneous ferroelectric polarization is about 26 μC cm^{-2} (REF.[147]), which are on the same order of magnitude as those of MXs. However, owing to the local field effect, perovskites will lose the polarization properties when thinned down into ultrathin films[148–150]. In MXs, because their polarization is along the in-plane direction, it is possible to maintain the polarization even in a monolayer.

The progress in the synthesis of MXs may enable the observation of many exciting phenomena in ferroelastics and multiferroics. In the future, identifying ferroelastic and ferroelectric domains will be a crucial challenge for understanding the transition dynamics and device performance of these materials. Realizing off-plane ferroelectricity is also interesting and important for broader applications. In addition, doping is predicted to be useful for realizing 2D magnetism[151,152]; thus, it may bring new magnetic order and further enrich multiferroics.

Perspectives

Although the research in BP, its isoelectronic MXs and other layered elemental and compound group V materials is still in its infancy, numerous new discoveries and device demonstrations are currently being made. For BP and other layered elemental and compound group V materials, probably the most urgent task is to develop and optimize large-scale synthesis approaches. For ultrathin films (<10 nm), surface passivation and encapsulation using high-quality dielectric are critical. Given the very different material properties of group V materials and dielectrics such as hBN, it may not be feasible to synthesize them directly in a layer-by-layer manner. As a result, one probably has to first synthesize ultrathin encapsulated amorphous materials and then leverage phase transitions induced by temperature, pressure and light to realize such materials. For MX, it is important to further develop the synthesis approaches for monolayers and characterize their ferroelectric and piezoelectric properties.

Looking forward, there are many interesting open questions. Can few-layer and thin-film BP or monolayer arsenic and antimony find applications in advanced electronics? Will BP or AsP and other alloys be incorporated in a mid-IR optoelectronic platform as alternative materials? Will monolayer or odd-layer MXs revolutionize piezoelectronics and ferroelectronics? Can tunable topology devices be realized experimentally in BP or alloys, and can novel application be enabled by these tunable topological properties? Further exploration of large-scale synthesis, material stability and fundamental properties under external stimuli of this group of materials with reduced symmetry should present a wide range of promising opportunities, not only for improving existing solid-state technologies but also for developing new device concepts.

Published online 8 April 2019

1. Bridgman, P. W. Two new modifications of phosphorus. *J. Am. Chem. Soc.* **36**, 1344–1363 (1914).
2. Morita, A. Semiconducting black phosphorus. *Appl. Phys. A* **39**, 227–242 (1986).
3. Novoselov, K. S. et al. Electric field effect in atomically thin carbon films. *Science* **306**, 666–669 (2004).
4. Novoselov, K. S. et al. Two-dimensional gas of massless Dirac fermions in graphene. *Nature* **438**, 197–200 (2005).
5. Zhang, Y., Tan, Y., W., Störmer, H. L. & Kim, P. Experimental observation of the quantum Hall effect and Berry's phase in graphene. *Nature* **438**, 201–204 (2005).
6. Novoselov, K. S. et al. Two-dimensional atomic crystals. *Proc. Natl. Acad. Sci.* **102**, 10451–10453 (2005).
7. Radisavljevic, B. et al. Single-layer MoS_2 transistors. *Nat. Nanotechnol.* **6**, 147–150 (2011).
8. Mak, K. F. et al. Atomically Thin MoS_2: A New Direct-Gap Semiconductor. *Phys.Rev. Lett.* **105**, 136805 (2010).
9. Splendiani, A. et al. Emerging Photoluminescence in Monolayer MoS_2. *Nano Lett.* **10**, 1271–1275 (2010).
10. Hunt, B. et al. Massive Dirac Fermions and Hofstadter butterfly in a van der Waals heterostructure. *Science* **340**, 1427–1430 (2013).
11. Xu, G., Zhang, Y., Duan, X., Balandin, A. A. & Wang, K. L. Variability effects in graphene: challenges and opportunities for device engineering and applications. *Proc. IEEE* **101**, 1670–1688 (2013).
12. Yu, Z. et al. Towards intrinsic charge transport in monolayer molybdenum disulfide by defect and interface engineering. *Nat. Commun.* **5**, 5290 (2014).
13. Xu, C. et al. Large-area high-quality 2D ultrathin Mo2C superconducting crystals. *Nat. Mater.* **14**, 1135–1141 (2015).
14. Kang, K. et al. High-mobility three-atom-thick semiconducting films with wafer scale homogeneity. *Nature* **520**, 656–660 (2015).
15. Desai, S. B. et al. MoS_2 transistors with 1-nanometer gate lengths. *Science* **354**, 99–102 (2016).
16. Liu, F. et al. Room-temperature ferroelectricity in $CuInP_2S_6$ ultrathin flakes. *Nat. Commun.* **7**, 12357 (2016).
17. Li, L. et al. Black phosphorus field-effect transistors. *Nat. Nanotechnol.* **9**, 372–377 (2014).
This paper demonstrates the first BP transistor.
18. Liu, H. et al. Phosphorene: an unexplored 2D semiconductor with a high hole mobility. *ACS Nano* **8**, 4033–4041 (2014).
This paper reported on monolayer black phosphorus and introduced "phosphorene". It also showed high hole mobility in thin-film BP.
19. Xia, F., Wang, H. & Jia, Y. Rediscovering black phosphorus as an anisotropic layered material for optoelectronics and electronics. *Nat. Commun.* **5**, 4458 (2014).
In this paper, black phosphorus was reintroduced as a layered thin-film material with anisotropic in-plane optical conductivity and Hall mobility.
20. Koenig, S. P., Doganov, R. A., Schmidt, H., Castro Neto, A. H. & Özyilmaz, B. Electric field effect in ultrathin black phosphorus. *Appl. Phys. Lett.* **104**, 103106 (2014).
21. Castellanos-Gomez, A. et al. Isolation and characterization of few-layer black phosphorus. *2D Mater.* **1**, 025001 (2014).
22. Rodin, A. S., Carvalho, A. & Castro Neto, A. H. Strain-induced gap modification in black black phosphorus. *Phys. Rev. Lett.* **112**, 176801 (2014).
23. Qiao, J., Kong, X., Hu, Z.-X., Yang, F. & Ji, W. High-mobility transport anisotropy and linear dichroism in few-layer black phosphorus. *Nat. Commun.* **5**, 4475 (2014).
24. Tran, V., Soklaski, R., Liang, Y. & Yang, L. Layer-controlled band gap and anisotropic excitons in few-layer black phosphorus. *Phys. Rev. B* **89**, 235319 (2014).
25. Rudenko, A. N. & Katsnelson, M. I. Quasiparticle band structure and tight-binding model for single and bilayer black phosphorus. *Phys. Rev. B* **89**, 201408 (2014).
26. Zhang, S. et al. Extraordinary photoluminescence and strong temperature/angle-dependent Raman responses in few-layer phosphorene. *ACS Nano* **8**, 9590–9596 (2014).
27. Wang, X. et al. Highly anisotropic and robust excitons in monolayer black phosphorus. *Nat. Nanotechnol.* **10**, 517–521 (2015).
28. Kim, J. et al. Observation of tunable band gap and anisotropic Dirac semimetal state in black phosphorus. *Science* **349**, 723–726 (2015).
29. Yuan, H. et al. Polarization-sensitive broadband photodetector using a black phosphorus vertical p–n junction. *Nat. Nanotechnol.* **10**, 707–713 (2015).
30. Youngblood, N., Chen, C., Koester, S. J. & Li, M. Waveguide-integrated black phosphorus photodetector with high responsivity and low dark current. *Nat. Photon.* **9**, 247–252 (2015).
31. Gillgren, N. et al. Gate tunable quantum oscillations in air-stable and high mobility few-layer phosphorene heterostructures. *2D Mater.* **2**, 011001 (2015).
32. Du, Y. et al. Auxetic black phosphorus: 2D material with negative Poisson's ratio. *Nano Lett.* **16**, 6701–6708 (2016).
33. Li, L. et al. Quantum Hall effect in black phosphorus two-dimensional electron system. *Nat. Nanotechnol.* **11**, 593–597 (2016).
This paper reported Quantum Hall Effect in thin-film black phosphorus.
34. Li, L. et al. Direct observation of the layer-dependent electronic structure in phosphorene. *Nat. Nanotechnol.* **12**, 21–25 (2017).
35. Deng, B. et al. Efficient electrical control of thin-film black phosphorus bandgap. *Nat. Commun.* **8**, 14474 (2017).
36. Cao, T., Li, Z., Qiu, Q. Y. & Louie, S. G. Gate switchable transport and optical anisotropy in 90o twisted bilayer black phosphorus. *Nano Lett.* **16**, 5542–5546 (2016).
37. Liu, Q., Zhang, X., Abdalla, L. B., Fazzio, A. & Zunger, A. Switching a normal insulator into a topological insulator via electric field with application to phosphorene. *Nano Lett.* **15**, 1222–1228 (2015).
This paper predicts the topological phase transition in biased BP.
38. Zhang, G. et al. Infrared fingerprints of few-layer black phosphorus. *Nat. Commun.* **8**, 14071 (2017).
39. Liu, Y. et al. Gate-tunable giant Stark effect in few-layer black phosphorus. *Nano Lett.* **17**, 1970–1977 (2017).
40. Singh, A. K. & Hennig, R. G. Computational prediction of two-dimensional group-IV mono-chalcogenides. *Appl. Phys. Lett.* **105**, 042103 (2014).
41. Gomes, L. C. & Carvalho, A. Phosphorene analogues: Isoelectronic two-dimensional group-IV monochalcogenides with orthorhombic structure. *Phys. Rev. B* **92**, 085406 (2015).
42. Shi, G. & Kioupakis, E. Anisotropic spin transport and strong visible-light absorbance in few-layer SnSe and GeSe. *Nano Lett.* **15**, 6926–6931 (2015).

43. Fei, R., Li, W., Li, J. & Yang, L. Giant piezoelectricity of monolayer group IV monochalcogenides: SnSe, SnS, GeSe, and GeS. *Appl. Phys. Lett.* **107**, 173104 (2015).
In this paper, giant piezoelectricity in monochalcogenides was predicted.
44. Fei, R., Kang, W. & Yang, L. Ferroelectricity and phase transitions in monolayer group-IV monochalcogenides. *Phys. Rev. Lett.* **117**, 097601 (2016).
45. Gomes, L. C., Carvalho, A. & Castro Neto A. H. Vacancies and oxidation of two-dimensional group-IV monochalcogenides. *Phys.Rev. B* **94**, 054103 (2016).
46. Rodin, A. S., Gomes, L. C., Carvalho, A. & Castro Neto, A. H. Valley physics in tin (II) sulfide. *Phys. Rev. B* **93**, 045431 (2016).
This paper predicted that equivalent valleys in monolayer tin sulfide can be selectively addressed by linear polarized light.
47. Hanakata., P. Z., Carvalho, A., Campbell, D. K. & Park, H. S. Polarization and valley switching in monolayer group-IV monochalcogenides. *Phys. Rev. B* **94**, 035304 (2016).
48. Wang, H. & Qian, X. Two-dimensional multiferroics in monolayer group-IV monochalcogenides. *2D Mater.* **4**, 015042 (2017).
49. Kamal, C. & Ezawa, M. Arsenene: two-dimensional buckled and puckered honeycomb arsenic systems. *Phys. Rev. B* **91**, 085423 (2015).
50. Zhu, Z., Guan, J. & Tománek, D. Strain-induced metal-semiconductor transition in monolayers and bilayers of gray arsenic: a computational study. *Phys. Rev. B* **91**, 161404 (2015).
51. Zhang, S. et al. Semiconducting group 15 monolayers: a broad range of band gaps and high carrier mobilities. *Angew. Chem.* **128**, 1698–1701 (2016).
52. Ji, J. et al. Two-dimensional antimonene single crystals grown by van der Waals epitaxy. *Nat. Commun.* **7**, 13352 (2016).
53. Pumera, M. & Sofer, Z. 2D monoelemental arsenene, antimonene, and bismuthene: beyond black phosphorus. *Adv. Mater.* **29**, 1605299 (2017).
54. Liu, B. et al. Black arsenic-phosphorus: layered anisotropic infrared semiconductors with highly tunable compositions and properties. *Adv. Mater.* **27**, 4423–4429 (2015).
55. Sofer, Z. et al. Layered black phosphorus: strongly anisotropic magnetic, electronic, and electron-transfer properties. *Angew. Chem. Int. Ed.* **55**, 3382–3386 (2016).
56. Mayorga-Martinez, C. C., Sofer, Z. & Pumera, M. Layered black phosphorus as a selective vapor sensor. *Angew. Chem. Int. Ed.* **54**, 14317–14320 (2015).
57. Liu, H., Du, Y., Deng, Y. & Ye, P. D. Semiconducting black phosphorus: synthesis, transport properties and electronic applications. *Chem. Soc. Rev.* **44**, 2732–2743 (2015).
58. Castellanos-Gomez, A. J. Black phosphorus: narrow gap, wide applications. *Phys. Chem. Lett.* **6**, 4280–4291 (2015).
59. Wang, X. & Lan, S. Optical properties of black phosphorus. *Adv. Opt. Photon.* **8**, 618–655 (2016).
60. Carvalho, A. et al. Phosphorene: from theory to applications. *Nat. Rev. Mater.* **1**, 16061 (2016).
61. Morita, A., Asahina, H., Kaneta, C. & Sasaki, T. *Proc. 17th Int. Conf. Phys. Semiconductors* (eds Chadi, J. D. & Harrison, W. A.) 1320–1324 (Springer, New York 1985).
62. Gaddemane, G. et al. Theoretical studies of electronic transport in mono- and bi-layer phosphorene: a critical overview. *Phys. Rev. B* **98**, 115416 (2018).
63. Long, G. et al. Achieving ultrahigh carrier mobility in two-dimensional hole gas of black phosphorus. *Nano Lett.* **16**, 7768–7773 (2016).
64. Kuriakose, S. et al. Effects of plasma-treatment on the electrical and optoelectronic properties of layered black phosphorus. *Appl. Mater. Today* **12**, 244–249 (2018).
65. Zhao, L.-D. et al. Ultralow thermal conductivity and high thermoelectric figure of merit in SnSe crystals. *Nature* **508**, 373–377 (2014).
66. Ballipinar, F. & Rastogi, A. Single-step organic vapor phase sulfurization synthesis of p-SnS photo-absorber for graded band-gap thin film heterojunction solar cells with n-$ZnO_{1-x}S_x$. *MRS Adv.* **1**, 2801–2806 (2016).
67. Xue, D. et al. GeSe thin-film solar cells fabricated by self-regulated rapid thermal sublimation. *J. Am. Chem. Soc.* **139**, 858–965 (2017).
68. Wang, G., Pandey, R. & Karna, S. P. Atomically thin group V elemental films: theoretical investigations of antimonene allotropes. *ACS Appl. Mater. Interfaces* **7**, 11490–11496 (2015).
69. Pizzi, G. et al. Performance of arsenene and antimonene double-gate MOSFETs from first principles. *Nat. Commun.* **7**, 12585 (2016).
70. Drozdov, I. K. et al. One-dimensional topological edge states of bismuth bilayers. *Nat. Phys.* **10**, 664–669 (2014).
71. Whitney, W. S. et al. Field effect optoelectronic modulation of quantum-confined carriers in black phosphorus. *Nano Lett.* **17**, 78–84 (2017).
72. Peng, R. et al. Mid-infrared electro-optic modulation in few-layer black phosphorus. *Nano Lett.* **17**, 6315–6320 (2017).
73. Lin, C., Grassi, R., Low, T. & Helmy, A. S. Multilayer black phosphorus as a versatile mid-infrared electro-optic materials. *Nano Lett.* **16**, 1683–1689 (2016).
74. Low, T. et al. Tunable optical properties of multilayer black phosphorus thin films. *Phys. Rev. B* **90**, 075434 (2014).
75. Xiang, Z. J. et al. Pressure-induced electronic transition in black phosphorus. *Phys. Rev. Lett.* **115**, 186403 (2015).
76. Fei, R., Tan, V. & Yang, L. Topologically protected Dirac cones in compressed bulk black phosphorus. *Phys. Rev. B.* **91**, 195319 (2015).
77. Gomes, L. C., Carvalho, A. & Castro Neto, A. H. Enhanced piezoelectricity and modified dielectric screening of two-dimensional group-IV monochalcogenides. *Phys. Rev. B* **92**, 214103 (2015).
78. Ziletti, A., Carvalho, A., Campbell, D. K., Coker, D. F. & Castro Neto, A. H. Oxygen defects in phosphorene. *Phys. Rev. Lett.* **114**, 046801 (2015).
In this paper, the oxidation effect of BP is investigated theoretically.
79. Favron, A. et al. Photooxidation and quantum confinement effects in exfoliated black phosphorus. *Nat. Mater.* **14**, 826–832 (2015).
80. Wood, J. D. et al. Effective passivation of exfoliated black phosphorus transistors against ambient degradation. *Nano Lett.* **14**, 6964–6970 (2014).
This paper demonstrates the effect passivation scheme of BP.
81. Cao, Y. et al. Quality heterostructures from two-dimensional crystals unstable in air by their assembly in inert atmosphere. *Nano Lett.* **15**, 4914–4921 (2015).
This paper shows the long-term stability of monolayer and few-layer BP encapsulated by hBN and reports on their transport properties.
82. Artel, V. et al. Protective molecular passivation of black phosphorus. *2D Mater. Appl.* **1**, 6 (2017).
83. Illarionov, Y. et al. Long-term stability and reliability of black phosphorus field-effect transistors. *ACS Nano* **10**, 9543–9549 (2016).
84. Jiang, J. et al. Two-step fabrication of single-layer rectangular SnSe flakes. *2D Mater.* **4**, 021026 (2017).
85. Hu, W. & Yang, J. Defects in phosphorene. *J. Phys. Chem. C.* **119**, 20474–20480 (2015).
86. Cai, Y., Ke, Q., Zhang, G., Yakobson, B. & Zhang, Y.-W. Highly itinerant atomic vacancies in phosphorene. *J. Am. Chem. Soc.* **138**, 10199–10206 (2016).
87. Köpf, M. et al. Access and in situ growth of phosphorene-precursor black phosphorus. *J. Cryst. Growth* **405**, 6–10 (2014).
88. Osters, O. et al. Synthesis and identification of metastable compounds: black arsenic-science or fiction? *Angew. Chem. Int. Ed.* **51**, 2994–2997 (2012).
89. Smith, J. B., Hagaman, D. & Ji, H. Growth of 2D black phosphorus film from chemical vapor deposition. *Nanotechnology* **27**, 215602 (2016).
90. Li, X. et al. Synthesis of thin-film black phosphorus on a flexible substrate. *2D Mater.* **2**, 1–6 (2015).
91. Yang, Z. et al. Field-effect transistors based on amorphous black phosphorus ultrathin films by pulsed laser deposition. *Adv. Mater.* **27**, 3748–3754 (2015).
92. Hanlon, D. et al. Liquid exfoliation of solvent-stabilized few-layer black phosphorus for applications beyond electronics. *Nat. Commun.* **6**, 8563 (2015).
93. Li, C. et al. Synthesis of crystalline black phosphorus thin film on sapphire. *Adv. Mater.* **30**, 1703748 (2018).
94. Sorgato, I., Guarise, G. B. & Marani, A. Red to black phosphorus transition up to 65 kbar. *High. Temp. High. Press.* **2**, 105–111 (1970).
95. Sun, Q. et al. Pressure quenching: a new route for the synthesis of black phosphorus. *Inorg. Chem. Front.* **5**, 669–674 (2018).
96. Jang, A.-R. et al. Wafer-scale and wrinkle-free epitaxial growth of single-orientated multilayer hexagonal boron nitride on sapphire. *Nano Lett.* **16**, 3360–3366 (2016).
97. Zhang, J. L. et al. Epitaxial growth of single layer blue phosphorus: a new phase of two-dimensional phosphorus. *Nano Lett.* **16**, 4903–4908 (2016).
98. Gao, J., Zhang, G. & Zhang, Y.-W. The critical role of substrate in stabilizing phosphorene nanoflake: a theoretical exploration. *J. Am. Chem. Soc.* **138**, 4763–4771 (2016).
99. Zhao, S. et al. Controlled synthesis of single-crystal SnSe nanoplates. *Nano Res.* **8**, 288–295 (2015).
100. Zhang, L. et al. Tinselenidene: a two-dimensional auxetic material with ultralow lattice thermal conductivity and ultrahigh hole mobility. *Sci. Rep.* **6**, 19830 (2016).
101. Li, L. et al. Single-layer single-crystalline SnSe nanosheets. *J. Am. Chem. Soc.* **135**, 1213–1216 (2013).
102. Chang, K. et al. Discovery of robust in-plane ferroelectricity in atomic-thick SnTe. *Science* **353**, 274–278 (2016).
103. Wang, H. et al. Black phosphorus radio-frequency transistors. *Nano Lett.* **14**, 6424–6429 (2014).
104. Zhu, W. et al. Flexible black phosphorus ambipolar transistors, circuits and AM demodulator. *Nano Lett.* **15**, 1883–1890 (2015).
105. del Alamo, J. A. Nanometre-scale electronics with III–V compound semiconductors. *Nature* **479**, 317–323 (2011).
106. Pillarisetty, R. Academic and industry research progress in germanium nanodevices. *Nature* **479**, 324–328 (2011).
107. Koenig, S. P. et al. Electron doping of ultrathin black phosphorus with Cu adatoms. *Nano Lett.* **16**, 2145–2151 (2016).
108. Prakash, A., Cai, Y., Zhang, G., Zhang, Y.-W. & Ang, K.-W. Black phosphorus N-type field-effect transistor with ultrahigh electron mobility via aluminum adatoms doping. *Small* **13**, 1602909 (2017).
109. Luo, X. et al. Continuous-wave and transient characteristics of phosphorene microwave transistors. *Dig. IEEE MTT-S Int. Microwave Symp.* https://doi.org/10.1109/MWSYM.2016.7540290 (2016).
110. Li, T. et al. Black phosphorus radio frequency electronics at cryogenic temperatures. *Adv. Electron. Mater.* **4**, 1800138 (2018).
111. Lundstrom, M. Elementary scattering theory of the Si MOSFET. *IEEE Electron Device Lett.* **18**, 361–363 (1997).
112. Dorgan, V. E., Bae, M. H. & Pop, E. Mobility and saturation velocity in graphene on SiO_2. *Appl. Phys. Lett.* **97**, 082112 (2010).
113. Chen, X. et al. Large-velocity saturation in thin-film black phosphorus transistors. *ACS Nano* **12**, 5003–5010 (2018).
114. Dean, C. R. et al. Boron nitride substrates for high-quality graphene electronics. *Nat. Nanotechnol.* **5**, 722–726 (2010).
115. Wang, L. et al. One-dimensional electrical contact to a two-dimensional material. *Science* **342**, 614–617 (2013).
116. Schwierz, F., Pezoldt, J. & Granzner, R. Two-dimensional materials and their prospects in transistor electronics. *Nanoscale* **7**, 8261–8283 (2015).
117. Sylvia, S. S. et al. Material selection for minimizing direct tunneling in nanowire transistors. *IEEE Trans. Electron Devices* **59**, 2064–2069 (2012).
118. Soref, R. Mid-infrared photonics in silicon and germanium. *Nat. Photon.* **4**, 495–497 (2010).
119. Buscema, M., Groenendijk, D. J., Steele, G. A., van der Zant, H. S. & Castellanos-Gomez, A. Photovoltaic effect in few-layer black phosphorus PN junctions defined by local electrostatic gating. *Nat. Commun.* **5**, 4651 (2014).
120. Long, M. et al. Room temperature high-detectivity mid-infrared photodetectors based on black arsenic phosphorus. *Sci. Adv.* **3**, e1700589 (2017).
121. Amani, M., Regan, E., Bullock, J., Ahn, G. H. & Javey, A. Mid-wave infrared photoconductors based on black arsenic phosphorus alloys. *ACS Nano* **11**, 11724–11731 (2017).
122. Miller, D. A. B. et al. Band-edge electroabsorption in quantum well structures: the quantum-confined Stark effect. *Phys. Rev. Lett.* **53**, 2173–2176 (1984).
123. Younis, U. et al. Germanium-on-SOI waveguides for mid-infrared wavelengths. *Opt. Express* **24**, 11987–11993 (2016).
124. Li, L. et al. Integrated flexible chalcogenide glass photonic devices. *Nat. Photon.* **8**, 643–649 (2014).
125. Kang, J., Takenaka, M. & Takagi, S. Novel Ge waveguide platform on Ge-on-insulator wafer for mid-infrared photonic integrated circuits. *Opt. Express* **24**, 11855–11864 (2016).

126. Deckoff-Jones, S. et al. Chalcogenide glass waveguide-integrated black phosphorus mid-infrared photodetectors. *J. Opt.* **20**, 044004 (2018).
127. Huang, L. et al. Waveguide-integrated black phosphorus photodetector for mid-infrared applications. *ACS Nano* **13**, 913–921 (2019).
128. Malik, A. et al. Germanium-on-silicon mid-infrared arrayed waveguide grating multiplexers. *IEEE Photon. Technol. Lett.* **25**, 1805–1808 (2013).
129. Martyniuk, P., Antoszewski, J., Martyniuk, M., Faraone, L. & Rogalski, A. New concepts in infrared photodetector designs. *Appl. Phys. Rev.* **1**, 041102 (2014).
130. Zhu, Z., Guan, J. & Tomanek, D. Structural transition in layered $As_{1-x}P_x$ compounds: a computational study. *Nano Lett.* **15**, 6042–6046 (2015).
131. Žutić, I., Fabian, J. & Das Sarma, S. Spintronics: fundamentals and applications. *Rev. Mod. Phys.* **76**, 323 (2004).
132. Qian, X., Liu, J., Fu, L. & Li, J. Quantum spin Hall Effect in two-dimensional transition metal dichalcogenides. *Science* **346**, 1344–1347 (2014).
133. Kim, J. et al. Two-dimensional Dirac Fermions protected by space-time inversion symmetry in black phosphorus. *Phys. Rev. Lett.* **119**, 226801 (2017).
134. Haleoot, R. et al. Photostrictive two-dimensional materials in the monochalcogenide family. *Phys. Rev. Lett.* **118**, 227401 (2017).
135. Lee, C., Wei, X., Kysar, J. W. & Hone, J. Measurement of elastic properties and intrinsic strength of monolayer graphene. *Science* **321**, 385–388 (2008).
136. Bertolazzi, S., Brivio, J. & Kis, A. Stretching and breaking of ultrathin MoS_2. *ACS Nano* **5**, 8703–9709 (2011).
137. Michel, K. H. & Verberck, B. Theory of elastic and piezoelectric effects in two-dimensional hexagonal boron nitride. *Phys. Rev. B* **80**, 224301 (2009).
138. Duerloo, K. N., Ong, M. T. & Reed, E. J. Intrinsic piezoelectricity in two-dimensional materials. *J. Phys. Chem. Lett.* **3**, 2871–2876 (2012).
139. Wu, W. Z. et al. Piezoelectricity of single-atomic-layer MoS_2 for energy conversion and piezotronics. *Nature* **514**, 470–474 (2014).
140. Zhu, H. et al. Observation of piezoelectricity in free-standing monolayer MoS_2. *Nat. Nanotechnol.* **10**, 151–155 (2015).
141. Schick, V. et al. Optical writing of magnetic properties by remanent photostriction. *Phys. Rev. Lett.* **117**, 107403 (2016).
142. Paillard, C., Xu, B., Dkhil, B., Geneste, G. & Bellaiche, L. Photostriction in ferroelectrics from density functional theory. *Phys. Rev. Lett.* **116**, 247401 (2016).
143. Wu, M. & Zeng, X. C. Intrinsic ferroelasticity and/or multiferroicity in two-dimensional phosphorene and phosphorene analogues. *Nano Lett.* **16**, 3236–3241 (2016).
144. Liu, C., Qin, H. & Mather, P. T. Review of progress in shape-memory polymers. *J. Mater. Chem.* **17**, 1543–1558 (2007).
145. Wang, H. & Qian, X. Giant optical second harmonic generation in two-dimensional multiferroics. *Nano Lett.* **17**, 5027–5034 (2017).
146. Safari, A. & Akdoğan, E. K. (eds) *Piezoelectric and Acoustic Materials for Transducer Applications* 17–38 (Springer, 2008).
147. Jaffe, B., Cook, W. R. Jr. & Jaffe, H. *Piezoelectric Ceramics*. (Academic Press, London, 1971).
148. Batra, I. P., Wurfel, P. & Silverman, B. D. New type of first-order phase transition in ferroelectric thin films. *Phys. Rev. Lett.* **30**, 384 (1973).
149. Zhong, W., King-Smith, R. D. & Vanderbilt, D. Giant LO-TO splitting in perovskite ferroelectrics. *Phys. Rev. Lett.* **72**, 3618 (1994).
150. Junquera, J. & Ghosez, P. Critical thickness for ferroelectricity in perovskite ultrathin films. *Nature* **422**, 506 (2003).
151. Seixas, L., Rodin, A. S., Carvalho, A. & Castro Neto, A. H. Multiferroic two-dimensional materials. *Phys. Rev. Lett.* **116**, 206803 (2016).
152. Cao, T., Li, Z. & Louie, S. G. Tunable magnetism and half-metallicity in hole-doped monolayer GaSe. *Phys. Rev. Lett.* **114**, 236602 (2015).

Acknowledgements
The authors dedicate this manuscript to the memory of their wonderful mentor and collaborator, Mildred Dresselhaus of Massachusetts Institute of Technology, USA, who passed away in the planning stage of this Review. The authors are deeply indebted to her for her guidance, encouragement and support since the very early stage of research on BP and its related materials. Her warmness, generosity, great vision and unfailing optimism in science will always be remembered. F.X. acknowledges the financial and/or technical support from the Office of Naval Research, National Science Foundation, Air Force Office of Scientific Research, IBM Corporation and Yale University. L.Y. is thankful for support from the National Science Foundation, Air Force Office of Scientific Research and Washington University in St Louis. H.W. acknowledges support from the Army Research Office, Army Research Laboratory, Air Force Office of Scientific Research, National Science Foundation, Northrop Grumman Corporation and University of Southern California. J.H. acknowledges support from the Office of Naval Research, Air Force Office of Scientific Research and National Science Foundation. The authors thank T.-P. Ma and Y. Zhou at Yale University for helpful discussions on black phosphorus transistor scaling and MX synthesis, respectively.

Author contributions
F.X. drafted the outline with inputs from H.W. and L.Y. F.X., L.Y. and H.W. co-wrote the manuscript. J.C.M.H. and A.H.C.N. provided comments and revised the manuscript.

Competing interests
F.X. has a pending patent application on the synthesis of encapsulated few-layer and thin-film black phosphorus and other group V compounds.

Publisher's note